

Observation of Distinct Electron-Phonon Couplings in Gated Bilayer Graphene

L. M. Malard, D. C. Elias, E. S. Alves, and M. A. Pimenta

Departamento de Física, Universidade Federal de Minas Gerais, 30123-970, Belo Horizonte, Brazil

(Received 14 August 2008; published 16 December 2008)

A Raman study of a back gated bilayer graphene sample is presented. The changes in the Fermi level induced by charge transfer splits the Raman G band, hardening its higher component and softening the lower one. These two components are associated with the symmetric (S) and antisymmetric vibration (AS) of the atoms in the two layers, the later one becoming Raman active due to inversion symmetry breaking. The phonon hardening and softening are explained by considering the selective coupling of the S and AS phonons with interband and intraband electron-hole pairs.

DOI: 10.1103/PhysRevLett.101.257401

PACS numbers: 78.30.Na, 63.20.kd, 81.05.Uw

The interaction of electrons and phonons is a fundamental issue for understanding the physics of graphene, resulting in the renormalization of phonon energy and the breakdown of the adiabatic (Born-Oppenheimer) approximation [1–4]. Although many new physical insights about the electron-phonon interaction were found in monolayer graphene [2–6], the bilayer graphene is a unique system to study distinct couplings between electrons and phonons that have different symmetries [7]. In this Letter we show that the application of a gate voltage in bilayer graphene splits the symmetric and antisymmetric optical phonon components, confirming a recent theoretical prediction for the distinct interactions of these phonons with intraband and interband electron-hole pairs [7]. This result is specially relevant since the development of bilayer graphene devices with tunable gap depends on the detailed understanding of the interaction between electrons and phonons in this material [8–10].

The zone center E_{2g} phonon mode of monolayer graphene, which gives rise to the Raman G band around 1580 cm^{-1} , exhibits a very strong coupling with electron-hole pairs. This interaction renormalizes the phonon energy $\hbar\omega_0$, giving rise to the so-called Kohn anomaly [1]. Moreover, theoretical models have predicted an interesting behavior for the phonon energy when the Fermi level ε_F is changed by varying the electron or hole concentration: the phonon energy softens logarithmically for values of the chemical potential smaller than half of the phonon energy, and it hardens otherwise. This hardening is ascribed to the suppression of the interaction between phonons and electron-hole pairs for $|\Delta\varepsilon_F| > \hbar\omega_0/2$. Besides this, an increase in either electron or hole density increases the phonon lifetime [2–6] due to the inhibition of the process of phonon decay into electron-hole pairs, thus reducing the G band linewidth. Recent Raman studies of monolayer graphene have confirmed the theoretical prediction concerning the hardening and narrowing of the G band, by doping the sample with electrons or holes [4–6].

In the case of bilayer graphene, the E_{2g} phonon mode splits into two components, associated with the symmetric (S) and antisymmetric (AS) displacements of the atoms in

the two layers. Moreover, due to the splitting of the π and π^* bands in this material, phonons can couple with electron-hole pairs produced in interband or intraband transitions. Ando [7] calculated recently the self-energy of the S and AS phonons for varying Fermi energies and predicted the hardening and softening of the S and AS phonons, respectively, induced by electron or hole doping. In this work we present experimental results that confirm the theoretical prediction by Ando [7], thus showing that the G band of bilayer graphene has indeed two components which exhibit opposite dependence as the Fermi level is tuned.

Figure 1(a) shows an optical microscope image of the bilayer graphene device obtained by exfoliating bulk graphite on a 300 nm thickness SiO_2 layer on the top of a heavily p doped Si substrate. An electrical contact was made by soldering an indium micro wire directly on the top of the flake [11]. Charge carriers were induced in the sample by applying a gate voltage V_g to the Si substrate with respect to the graphene contact. The Raman measurements were carried out at room temperature using a triple Dilor XY spectrometer with a resolution smaller than 1 cm^{-1} , an 80x objective with spot size of $\sim 1\text{ }\mu\text{m}$ and the 2.41 eV laser excitation with 1 mW power. The number of layers in our graphene sample was determined by analyzing the shape of the G' (or 2D) band around $\sim 2700\text{ cm}^{-1}$ [Fig. 1(b)], which is composed of four peaks and exhibits a typical shape of a bilayer graphene [12–15].

Figure 1(c) shows the Raman spectra taken at different values of V_g . We observe that both the position and the shape of the G band depend on V_g , in agreement with previous Raman studies of gated bilayer graphene [16,17]. However, in our experiment we were not able to observe the initial softening of the G band for $|\varepsilon_F| < \hbar\omega_G/2$, as reported by Yan *et al.* [16]. This result can be explained by the presence of a larger nonhomogeneous charge distribution in our sample and by the fact that our experiment was done at room temperature.

Figure 2(a) shows the fittings of the Raman G band of the bilayer graphene device for different values of V_g . The G bands observed in the spectra taken at V_g equals to -80 ,

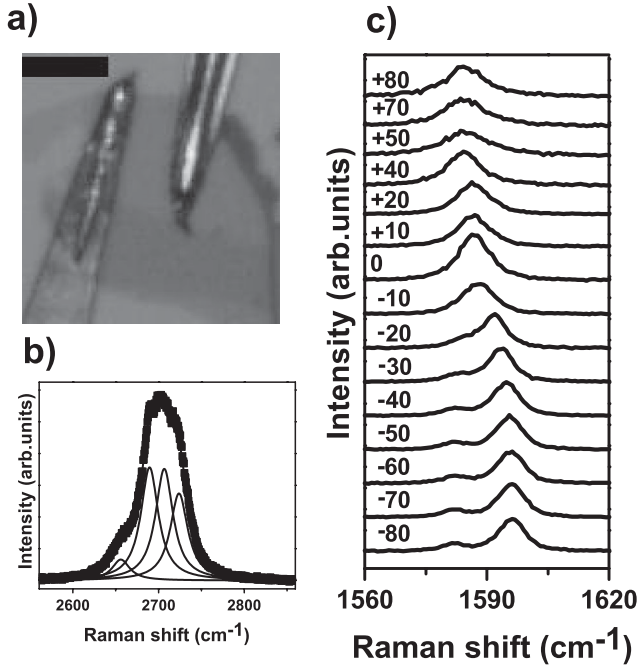


FIG. 1. (a) Optical microscope image of gated graphene bilayer sample (the scale bar is 15 μm). (b) Raman spectrum of the G' band of bilayer graphene. (c) Raman spectrum of the G band for different values of V_g .

-40, and -20 V clearly exhibit two peaks. All spectra taken at positive values of gate voltage could be fitted by a single Lorentzian.

Figures 3(a) and 3(b) show the relative shift (with respect to G band position in the +50 V spectrum) and the full width at half maximum (FWHM) of the Lorentzians that fit the G band as a function of the applied gate voltage, respectively. Notice that the frequency of the high energy component increases with decreasing values of V_g , whereas the opposite behavior is observed for the low

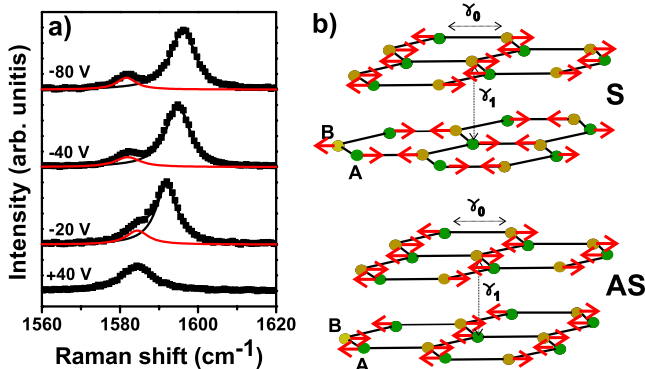


FIG. 2 (color online). (a) Raman G band of the bilayer graphene for -80 V, -40 V, -20 V and +40 V gate voltages. Two Lorentzian curves are needed to fit the G band for -80, -40, and -20 V. (b) Displacement of the atoms for the S and AS highest energy phonon modes in the Γ point of bilayer graphene.

energy component. Figure 3(b) shows that the FWHM exhibits a maximum for $V_g = +50$ V spectrum, and it clearly decreases with decreasing values of V_g .

Let us discuss the origin of the two peaks that compose the G band shown in Fig. 2(a). The bilayer graphene is formed by two graphene layers in the AB Bernal stacking, where the point group at Γ point is D_{3d} . The phonon branch associated with the E_{2g} mode of monolayer graphene gives rise to two branches for bilayer graphene, one S and other AS (in-phase and out-of-phase displacements of the atoms in the two layers), which are represented at Fig. 2(b). At the center of the Brillouin zone (Γ point), the S and AS vibrations belong to the two doubly degenerated representations E_g and E_u , respectively. The antisymmetric E_u mode is not Raman active since the D_{3d} group is centrosymmetric. However, if the inversion symmetry operation of the bilayer graphene is broken, the system is described by the C_{3v} point group at the Γ point. In this case, both the S and the AS modes belong to the E representation, and are Raman active.

The inversion symmetry breaking can be due to the different materials that the top and bottom graphene layers of our device are exposed to and/or to a nonhomogeneous

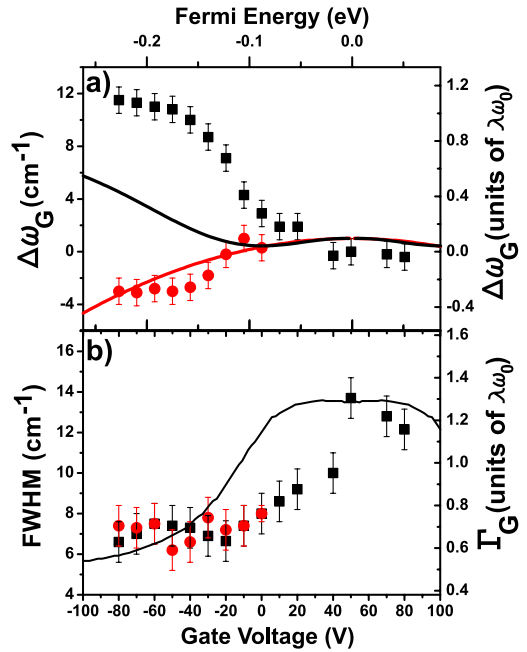


FIG. 3 (color online). (a) The black squares and red circles correspond to the relative shift ($\Delta\omega_G$) of the S and AS components of the G band, respectively, with respect to the position in the +50 V spectrum, as a function of the applied gate voltage (bottom scale). The solid curves corresponds to the theoretical prediction for the relative G band shift [7] in units of $\lambda\omega_0$ as a function of the Fermi energy (top scale). (b) The black squares and red circles correspond to the FWHM of the S and AS components of the G band, respectively, and the solid curve corresponds to the theoretical prediction for the FWHM of the symmetric phonon mode [7].

doping of the top and bottom layers. The nonequivalence between the top and bottom layers decreases the symmetry, making the antisymmetric mode active in the Raman spectra, explaining thus the two components of the G band. The energy separation between the S and AS components is negligible when the Fermi level is close to the Dirac point, and this can be seen in the spectrum taken at +40 gate voltage in Fig. 1(b). However, the doping with electrons or holes induces a measurable energy splitting for those components, as shown in the spectra between -20 to -80 V in Fig. 1(b).

One could argue that the observed splitting of the G band is related to the symmetric mode coming from the top and bottom layers, in the case of a nonhomogeneous doping of the two layers. However, this interpretation has serious drawbacks in the present case. Notice that the low energy component of the G band is about 5 times less intense than the higher energy one. Considering that the transmittance of visible light in monolayer graphene is about 97.7% [18], the contributions of the symmetric mode from the upper and bottom layers for the Raman scattering are expected to be almost the same. Furthermore, our results show that the energy of the low energy component decreases when the Fermi level is changed. This result would not be expected if one associates the lower energy Raman peak with the symmetric mode of the bilayer graphene bottom layer. We stress the fact that the splitting of the G band was not reported in the two recent studies of gated bilayer graphene devices [16,17], despite the fact that the G band observed in reference [16] is clearly asymmetric. Possibly our observation of this splitting is due to the characteristic of our device, which leads to the inversion symmetry breaking and allows the observation of the nonactive Raman AS vibration.

In order to discuss the phonon renormalization effect in bilayer graphene, we must consider the selection rules for the interaction of the S and AS phonons with the interbands or intrabands electron-hole pairs. The band structure of bilayer graphene near the K point shown in Fig. 4 consists of four parabolic bands, two of them touch each other at the K point, and the other two bands separated by $2\gamma_1$, where $\gamma_1 \sim 0.35$ eV. The electron-phonon interaction in bilayer graphene is described by a 2×2 matrix for each phonon symmetry, where each matrix element gives the contribution of electron-hole pairs involving different electronic sub-bands [7]. For the S phonon mode, all matrix elements are different from zero, and this phonon can interact with both interband or intraband electron-hole pairs, as shown in Fig. 4(a), giving rise to the phonon energy renormalization (Kohn anomaly). However, for the AS phonon mode, the diagonal terms of the matrix are null, showing that there is no coupling between AS phonons and interband electron-hole pairs. Therefore, no Kohn anomaly is expected for the antisymmetric phonon mode when the Fermi level is at the Dirac point.

However, if the Fermi energy is changed [for instance, $\varepsilon_F < 0$ as shown in Fig. 4(b)], intraband electron-hole

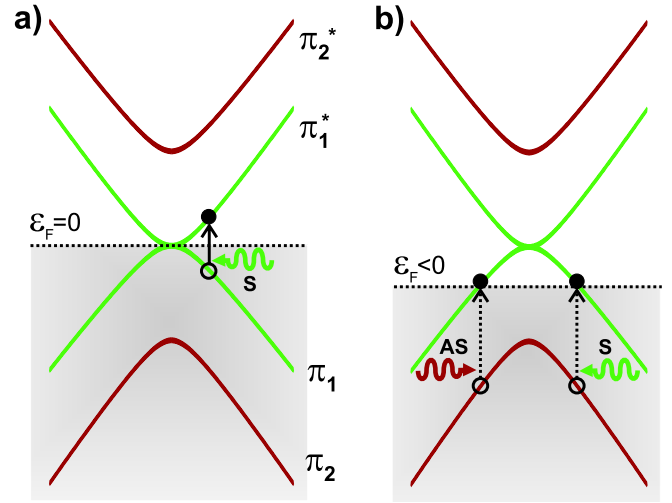


FIG. 4 (color online). Parabolic band structure of bilayer graphene near the K point. The vertical arrows illustrates the possible transitions induced by symmetric (green) and antisymmetric (red) $\mathbf{q} = 0$ phonons for (a) interband electron-hole pairs creation at ($\varepsilon_F = 0$) and (b) intraband electron-hole pairs creation ($\varepsilon_F < 0$). The gap opening is not considered in this diagram.

pairs can be produced by phonons. Now, the AS phonons have also their energies renormalized, giving rise to the Kohn anomaly. Notice that as the energy separation between the π_1 and π_2 bands ($\gamma_1 \sim 0.35$ eV) is larger than the G band energy (~ 0.2 eV), the electron-hole pairs creation by those phonons is a virtual process. Therefore, we expect the dependence of the shift of the antisymmetric mode with Fermi energy to be smoother than that of the symmetric mode. A similar result has been recently observed in gated semiconducting carbon nanotubes [19] which have the band gap larger than the phonon energy.

In order to explain our experimental results, we have also plotted in Figs. 3(a) and 3(b) frequency shift and broadening (FWHM) of the G band calculated by T. Ando [7] as $\Delta\omega_G = \text{Re}[\Pi^{(\pm)}(\omega)]$ and $\Gamma_G = -2\text{Im}[\Pi^{(\pm)}(\omega)]$ [17], respectively, where Π is the phonon self-energy given of the symmetric (+) or antisymmetric (-) components, given by :

$$\Pi^{(\pm)}(\omega) = -\lambda \int_0^\infty \gamma^2 k dk \sum_{j,j'} \sum_{s,s'} \Phi_{jj'}^{(\pm)} \times \frac{[f(\varepsilon_{sjk}) - f(\varepsilon_{s'j'k'})](\varepsilon_{sjk} - \varepsilon_{s'j'k'})}{(\hbar\omega + i\delta)^2 - (\varepsilon_{sjk} - \varepsilon_{s'j'k'})^2}. \quad (1)$$

The functions ε_{sjk} are the electronic band dispersions (k is the modulus of the wave vector), $s = +1$ and -1 denotes the conduction and valence bands, respectively, and $j = 1, 2$ specifies the two bands within the valence and conduction bands. The function $f(\varepsilon_{sjk})$ is the Fermi distribution and the matrix elements $\Phi_{jj'}^{(\pm)}(k)$ gives the relative contribution of the S (+) and AS (-) phonons for the interband and intraband electron-hole pairs formed in transitions [7].

The phenomenological damping parameter δ in Eq. (1) describes the charge inhomogeneity in the sample and washes out the logarithmic singularity present at $\varepsilon_F = \hbar\omega_0/2$. We have considered the value of $\delta = 0.1$ eV in the theoretical curves depicted in Fig. 3, since this is the smallest value of δ necessary to remove the initial phonon softening for $\varepsilon_F < \hbar\omega_0/2$ [2,7].

Theoretical curves $\Delta\omega_G$ and Γ_G are calculated in units of $\lambda\omega_0$, where $\omega_0 = 0.196$ eV is the energy of the optical phonon and λ is related to the strength of the electron-phonon coupling and given by [7]:

$$\lambda = 0.16 \times 10^{-3} (\text{\AA}^2 \text{eV}^{-2}) \left[\frac{\partial\gamma_0}{\partial b} \right]^2, \quad (2)$$

where γ_0 is the in-plane nearest-neighbor tight-binding parameter [see Fig. 2(b)] and b is the C-C distance.

In order to compare the experimental and theoretical results depicted in Figs. 3(a) and 3(b) we need to convert the experimental horizontal scale (applied gate voltage, in the bottom axis of Fig. 3) into the theoretical scale (Fermi energy, in the upper axis of Fig. 3), and the experimental vertical scales (in cm^{-1} , left-side axes of Fig. 3) into the theoretical scales (in units of $\lambda\omega_0$, right-side axes of Fig. 3).

To match the scales of the experimental (left axis) and calculated (right axis) values of $\Delta\omega_G$ and Γ_G , shown in Fig. 3, we have used the value $\partial\gamma_0/\partial b = 6.4$ eV \AA^{-1} in Eq. (2) [20]. Both theoretical curves $\Delta\omega_G$ and Γ_G are plotted in Fig. 3 as a function of the Fermi energy ε_F (top axis), while the experimental values are plotted as a function of gate voltage (bottom axis). In order to scale these axes, we have used the fact that both ε_F and V_g are related to the electron (or hole) density n , which is assumed to be the same in both layers. The modulus of the Fermi energy $|\varepsilon_F|$ is related to the electron (or hole) density in the regime $|\varepsilon_F| < \gamma_1$ by [7]:

$$|\varepsilon_F| = \frac{1}{2}(-\gamma_1 + \sqrt{4n\pi\gamma^2 + \gamma_1^2}), \quad (3)$$

where $\gamma = \frac{\sqrt{3}}{2}a\gamma_0$, $a = 2.46$ \AA is the lattice constant, $\gamma_0 \approx 3$ eV and $\gamma_1 \sim 0.35$ eV is the out-of-plane nearest-neighbor parameter [see Fig. 2(b)]. A parallel plate capacitor model gives $n = 7.2 \times 10^{10} \text{ cm}^{-2} \text{ V}^{-1} (V_g - V_D)$, where V_D is the gate voltage needed to move the Fermi level to the Dirac point due to intrinsic doping of the sample. The value of $V_D = +50$ V was obtained from the spectrum where the G band has the largest FWHM [see Fig. 3(b)], since the symmetric phonon lifetime is minimum for $\varepsilon_F = 0$ [7].

Figure 3 shows that there is a qualitative agreement between our experimental results and the theoretical prediction of the dependence of the frequency and width of the symmetric and antisymmetric optical phonons in bilayer

graphene with the Fermi level. We shall stress that this good agreement is obtained despite the different approximations that have been done. Notice first that the theoretical model does not take into account the trigonal warping effect, the angular dependence of the electron-phonon coupling, and the strength $\partial\gamma_1/\partial b$ for the coupling between electrons and AS phonons [see Fig. 2(b)]. Moreover, we have used the simple model of a parallel capacitor with homogeneous carrier concentration in the two layers. A more complete model is needed to improve the fitting of the experimental data.

In summary, we have shown in this work that bilayer graphene is a unique material where the phonon renormalization tuned by charge transfer depends strongly on the symmetry of the phonons involved in the creation of electron-hole pairs. The hardening of the S mode and the softening of the AS phonon mode is explained by the creation of interband or intrabands electron-hole pairs by S and AS optical phonons, giving an experimental support for the theoretical predictions of the optical phonons dependence on charge concentration in bilayer graphene [7].

We acknowledge useful discussions with R. Saito, A. H. Castro Neto, and K. S. Novoselov. The graphite sample used to prepare the exfoliated graphene was provided by Nacional de Grafite (Brazil). This work was supported by Rede Nacional de Pesquisa em Nanotubos de Carbono - MCT and FAPEMIG and CNPq.

-
- [1] S. Piscanec *et al.*, Phys. Rev. Lett. **93**, 185503 (2004).
 - [2] T. Ando, J. Phys. Soc. Jpn. **75**, 124701 (2006).
 - [3] M. Lazzeri and F. Mauri, Phys. Rev. Lett. **97**, 266407 (2006).
 - [4] S. Pisana *et al.*, Nature Mater. **6**, 198 (2007).
 - [5] J. Yan *et al.*, Phys. Rev. Lett. **98**, 166802 (2007).
 - [6] A. Das *et al.*, Nature Nanotech. **3**, 210 (2008).
 - [7] T. Ando, J. Phys. Soc. Jpn. **76**, 104711 (2007).
 - [8] A. H. Castro Neto *et al.*, arXiv:cond-mat/0709.1163. [Rev. Mod. Phys. (to be published)].
 - [9] J. B. Oostinga *et al.*, Nature Mater. **7**, 151 (2008).
 - [10] E. V. Castro *et al.*, Phys. Rev. Lett. **99**, 216802 (2007).
 - [11] Ç. Ö. Girit and A. Zettl, Appl. Phys. Lett. **91**, 193512 (2007).
 - [12] A. C. Ferrari *et al.*, Phys. Rev. Lett. **97**, 187401 (2006).
 - [13] A. Gupta *et al.*, Nano Lett. **6**, 2667 (2006).
 - [14] D. Graf *et al.*, Nano Lett. **7**, 238 (2007).
 - [15] L. M. Malard *et al.*, Phys. Rev. B **76**, 201401 (2007).
 - [16] J. Yan *et al.*, Phys. Rev. Lett. **101**, 136804 (2008).
 - [17] A. Das *et al.*, arXiv:0807.1631v1.
 - [18] R. R. Nair *et al.*, Science **320**, 1308 (2008).
 - [19] J. C. Tsang *et al.*, Nature Nanotech. **2**, 725 (2007).
 - [20] A. H. Castro Neto and F. Guinea, Phys. Rev. B **75**, 045404 (2007).